Structure and Behavior of Triad Interactions for a Boussinesq System Arising in a Model for the Formation Sand Ridges

Juan Mario Restrepo

Mathematics and Computer Science Division

Argonne National Laboratory, Argonne IL U.S.A. 60439

Jerry L. Bona

Mathematics Department

The Pennsylvania State University, University Park PA U.S.A. 16802

Preprint MCS-P409-1293,

Mathematics and Computer Science Division

Argonne National Laboratory, Argonne, IL, 1993

Abstract

The Boussinesq system describes weakly nonlinear dispersive long waves in plasmas and incompressible irrotational fluids. This study presents some results regarding the structure and behavior of a system of equations that yield the spatial structure of triad interactions in the Boussinesq system. Such a system forms part of a model for the formation and evolution of sand ridges on the continental shelf. The aims of this study are to provide some insight into the behavior of the triad system and into the sand ridge model in particular.

1 Introduction

A model for the formation and evolution of three-dimensional longshore sand ridges on the continental shelf was proposed in [1] and [2]. It identifies weakly nonlinear, dispersive shallow-water waves as the agents of formation of these structures. It is assumed that the waves travel mainly perpendicular to the shore (i.e., in the x direction) and have weak spanwise y dependence, thus

$$y \leftarrow \alpha^{1/2} y \qquad \hat{y}\cdot\mathbf{u} \leftarrow \alpha^{-1/2}\hat{y}\cdot\mathbf{u}. \tag{1}$$

These waves, for bottom topographies $h = 1+\varepsilon f(xy)$ with very slight slope changes (i.e., $\varepsilon \ll 1$), are governed by the dimensionless regularized Boussinesq system

$$\begin{aligned} \eta_t + \nabla\cdot[(h+\alpha\eta)\mathbf{u}] - \frac{1}{3}\beta^2\nabla\cdot[\nabla(h^2\eta_t)] &= 0 \\ \mathbf{u}_t + \alpha(\mathbf{u}\cdot\nabla)\mathbf{u} + \nabla\eta &= 0, \end{aligned} \tag{2}$$

where $\eta(x,y)$ is the amplitude and $\mathbf{u}(x,y)$ is the velocity of the water waves. The parameters $\alpha \ll 1$ and $\beta^2 \ll 1$ are the degree of nonlinearity and dispersion in the waves, respectively. The bottom evolution is given by

$$\begin{aligned} \frac{\partial}{\partial T}h(x,y,T) &= \tfrac{K}{\rho_0}(U_x + V_y) \\ h(x,y,0) &= \mathcal{H}(x,y), \end{aligned} \tag{3}$$

where U and V are the longshore and spanwise drift velocity components in the boundary layer and are themselves functions of the water wave amplitude.

In order to study the model's behavior and predictive qualities, the dynamics of

the surface waves were simplified by assuming a crude but still very usefull ansatz

$$\begin{aligned} u(x,X,y,t) &= \textstyle\sum_{j=1}^{2}[a_j(X,y)+\alpha A_j(X,y)]e^{i(k_jx-\omega_jt)}+c.c. \\ &\quad +\textstyle\sum_{j=1}^{2}[b_j(X,y)+\alpha B_j(X,y)]e^{i(-k_jx-\omega_jt)}+c.c., \end{aligned} \tag{4}$$

where c.c. stands for complex conjugate of the expression immediately preceding its appearance. The a's are the complex incident wave amplitudes, and the b's are the complex reflected wave amplitudes. The reality of the physical variables implies that $a_{-j}=a_j^\star$ and $b_{-j}=b_j^\star$. The spanwise velocity at the surface is

$$\begin{aligned} v(x,X,y,t) &= \textstyle\sum_{j=1}^{2}-\frac{i}{k_j}[a_{jy}(X,y)+O(\alpha)]e^{i(k_jx-\omega_jt)}+c.c. \\ &\quad +\textstyle\sum_{j=1}^{2}-\frac{i}{k_j}[b_{jy}(X,y)+O(\alpha)]e^{i(-k_jx-\omega_jt)}+c.c. \end{aligned} \tag{5}$$

To lowest order, $u_{0t}+\eta_{0x}=0$. Hence, an expression for the surface amplitude is readily available:

$$\begin{aligned} \eta_0 &= \sum_{j=1}^{\infty}\frac{\omega_j}{k_j}[a_j(X,y)+\alpha A_j(X,y)]e^{i(k_jx-\omega_jt)}+c.c. \\ &\quad +\sum_{j=1}^{\infty}\frac{\omega_j}{k_j}[b_j(X,y)+\alpha B_j(X,y)]e^{i(-k_jx-\omega_jt)}+c.c. \end{aligned} \tag{6}$$

A solution of the form given by Equations (4), (5), and (6) is valid, provided that the following relation holds between the frequency ω and the wavenumber k:

$$\omega_j^2-\frac{k_j^2}{1+\beta^2\frac{k_j^2}{3}}=0, \tag{7}$$

which gives the dispersion relation for the j-th mode, the positive root k_j corresponding to the shoreward-directed wave, and the negative to the seaward wave.

In addition, a compatibility condition must be satisfied, which then yields the equations for the spatial evolution of the surface modes, namely,

$$\begin{aligned}
a_{1x} - iK_1 a_{1yy} + iK_3 f(x,y) a_1 + iK_5 e^{-i\delta x} a_1^\star a_2 &= 0 \\
a_{2x} - iK_2 a_{2yy} + iK_4 f(x,y) a_2 + iK_6 e^{+i\delta x} a_1^2 &= 0 \\
b_{1x} + iK_1 b_{1yy} - iK_3 f(x,y) b_1 - iK_5 e^{+i\delta x} b_1^\star b_2 &= 0 \\
b_{2x} + iK_2 b_{2yy} - iK_4 f(x,y) b_2 - iK_6 e^{-i\delta x} b_1^2 &= 0 \\
a_1(x=0,y) &= \mathcal{A}_1(y) \\
a_2(x=0,y) &= \mathcal{A}_2(y) \\
b_1(x=M,y) &= \mathcal{B}_1(y) \\
b_2(x=M,y) &= \mathcal{B}_2(y)
\end{aligned} \tag{8}$$

plus appropriate boundary conditions on $y = 0$ and $y = N$. The real K and L constant coefficients are $O(\alpha, \varepsilon)$; they are described in [1] and [2] and given in the appendix. The real parameter $\delta \leq 0$ is the detuning from perfect resonance, that is, $\omega_2 = 2\omega_1$ and $k_2 = 2k_1 - \delta$.

If the boundary conditions $\mathcal{B}_1$ and $\mathcal{B}_2$ of the reflected wave are small, the reflected component is negligible. The triad system is then

$$\begin{aligned}
a_{1x} - iK_1 a_{1yy} + iK_3 f(x,y) a_1 + iK_5 e^{-i\delta x} a_1^\star a_2 &= 0 \\
a_{2x} - iK_2 a_{2yy} + iK_4 f(x,y) a_2 + iK_6 e^{+i\delta x} a_1^2 &= 0 \\
a_1(x=0,y) &= \mathcal{A}_1(y) \\
a_2(x=0,y) &= \mathcal{A}_2(y).
\end{aligned} \tag{9}$$

This study is devoted to the formal and analytical results relevant to discerning

the behavior and structure of the triad system, Equation (9). Although the linear part of the triad system is similar to its counterpart in the nonlinear Schrödinger equation, the nonlinear terms endow the Equation (9) with properties and behavior much unlike the nonlinear Schrödinger equation.

To give the reader an idea of the rich structure of the triad system, we solve Equation (9) in the following examples using periodic boundary conditions in y. The bottom is flat in all the examples; that is, $f(x,y) = 0$. The graphs were generated by using the fixed-point method [3], in which the linear operator is discretized using the Douglas scheme. The discretization yields a Jacobi matrix. In the graphs, two periods in y are plotted in tandem, the calculation being performed on only one of the two periods. The domain has $M = 240$ and $N = 150$, where M and N are respectively the length in x and breadth in y, and the fundamental frequency used was $\omega_1 = 1.2$. The parameters were $\alpha = 0.1$ and $\beta = 0.18$. The solution to the case with boundary conditions $\mathcal{A}_1 = 0.5 + 0.1\sin(\frac{3}{N}\pi y)$ and $\mathcal{A}_2 = 0$, with $\delta \neq 0$, is illustrated in Figure 1. For the same parameters, but with the boundary condition $\mathcal{A}_1 = 0.1\sin(\frac{3}{N}\pi y)$, the outcome is shown in Figure 2. Figure 3 shows the outcome when δ has been forced to zero. Finally, Figure 4 illustrates the case with quasi-periodic boundary conditions $\mathcal{A}_1 = 0.1[\sin(\frac{3}{N}\pi y) + \sin(\frac{8}{N}\pi y)]$ and $\mathcal{A}_2 = 0$, with the same parameter values as in Figure 3, except that $\delta \neq 0$. The numerical solution of these examples suggest that solutions to the triad system may be stable and periodic.

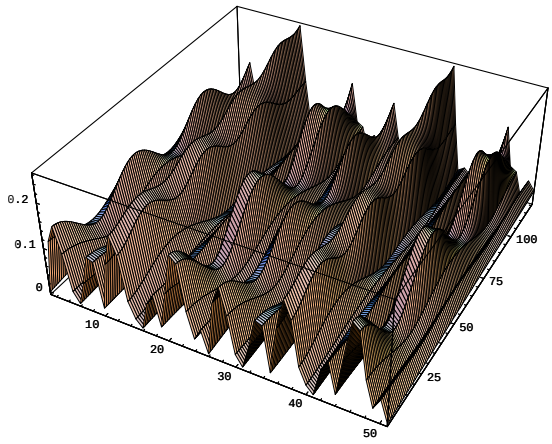

Figure 1: $a_1(x,y)$ for $\mathcal{A}_1 = 0.5 + 0.1\sin(\frac{3}{N}\pi y)$, $\mathcal{A}_2 = 0$, and $\delta \neq 0$.

2 Hamiltonian Structure of the Triad System

We adopt the following scaling,

$$\begin{array}{lll} x \leftarrow K_5(K_6E_0)^{1/2}x & y \leftarrow K_5^{1/2}(K_6E_0)^{1/4}y & \Delta Q \leftarrow \frac{\delta}{K_5(K_6E_0)^{1/2}} \\ u \leftarrow \frac{\sqrt{2}a_1}{(K_5E_0)^{1/2}} & v \leftarrow \frac{\sqrt{2}a_2}{(K_6E_0)^{1/2}}, & \end{array} \tag{10}$$

in order to facilitate the derivation of the Hamiltonian structure of the triad systems. With compact support in the y direction for both u and v and a flat bottom (i.e., $h = 1$), the system is

$$\begin{aligned} u_x - iK_1u_{yy} + ie^{-i\Delta Q x}u^\star v &= 0 \\ v_x - iK_2v_{yy} + ie^{+i\Delta Q x}u^2/2 &= 0. \end{aligned} \tag{11}$$

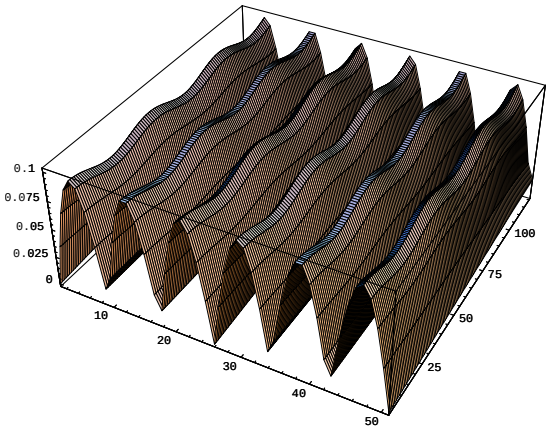

Figure 2: $a_1(x,y)$ for $\mathcal{A}_1 = 0.1\sin(\frac{3}{N}\pi y)$, $\mathcal{A}_2 = 0$, and $\delta \neq 0$.

The Lagrangian density is found to be

$$\mathcal{L} = iu_x u^\star - iu_x^\star u + iv_x v^\star - iv_x^\star v - \Re[(u^\star)^2 v e^{-i\Delta_Q x}] - K_1|u_y^2| - K_2|v_y^2|, \qquad (12)$$

where $\Re$ stands for "the real part of", and the canonical momenta are

$$\begin{aligned} \Pi_1 &= \frac{\partial \mathcal{L}}{\partial_{u_x}} = iu^\star \\ \Pi_2 &= \frac{\partial \mathcal{L}}{\partial_{v_x}} = iv^\star \\ \Pi_1^\star &= \frac{\partial \mathcal{L}}{\partial_{u_x^\star}} = iu \\ \Pi_2^\star &= \frac{\partial \mathcal{L}}{\partial_{v_x^\star}} = iv. \end{aligned} \qquad (13)$$

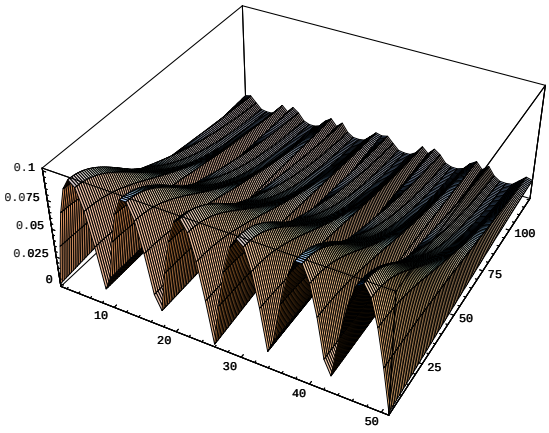

Figure 3: $a_1(x,y)$ for boundary conditions $\mathcal{A}_1 = 0.1\sin(\frac{3}{N}\pi y)$, $\mathcal{A}_2 = 0$, and detuning parameter $\delta = 0$.

The requirement that $L = \int \mathcal{L} dy$ be stationary yields the Euler-Lagrange equations, which in turn lead to (11):

$$\begin{aligned} \frac{\partial \mathcal{L}}{\partial u^\star} - \frac{d}{dy}\frac{\partial \mathcal{L}}{\partial u^\star_y} &= iu_x + K_1 u_{yy} - e^{-i\Delta_{Qx}} u^\star v &= 0 \\ \frac{\partial \mathcal{L}}{\partial v^\star} - \frac{d}{dy}\frac{\partial \mathcal{L}}{\partial v^\star_y} &= iv_x + K_2 v_{yy} - e^{+i\Delta_{Qx}} u^2/2 &= 0 \end{aligned} \tag{14}$$

and its complex conjugates. The Hamiltonian H and its density $\mathcal{H}$ are given by

$$\begin{aligned} H &= \int \mathcal{H} dy \\ \mathcal{H} &= \Re[(u^\star)^2 v e^{-i\Delta_{Qx}}] + K_1 |u_y|^2 + K_2 |v_y|^2. \end{aligned} \tag{15}$$

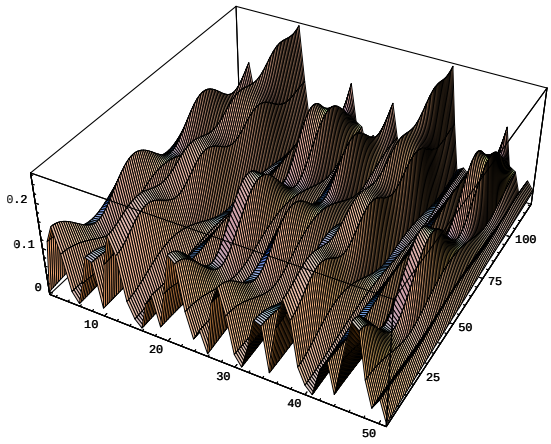

Figure 4: Solution for quasi-periodic boundary conditions: $\mathcal{A}_1 = 0.1[\sin(\frac{3}{N}\pi y) + \sin(\frac{8}{N}\pi y)]$, and $\mathcal{A}_2 = 0$. $\delta \neq 0$.

Note that the Hamiltonian is not conserved, that is,

$$\frac{\partial L}{\partial x} = -\frac{\partial H}{\partial x} \neq 0, \tag{16}$$

except when $\Delta Q = 0$. The Hamiltonian, in terms of the conjugate momenta, is

$$\mathcal{H} = -i\Re[\Pi_1^2 \Pi_2^\star e^{-i\Delta_Q x}] + K_1 |\Pi_{1y}|^2 + K_2 |\Pi_{2y}|^2. \tag{17}$$

The Hamiltonian admits a Poisson structure, defining the Poisson bracket as

$$\{A, B\} \equiv \int dy [\frac{\partial A}{\partial u}\frac{\partial B}{\partial \Pi_1} - \frac{\partial A}{\partial \Pi_1}\frac{\partial B}{\partial u}] + c.c. + \int dy [\frac{\partial A}{\partial v}\frac{\partial B}{\partial \Pi_2} - \frac{\partial A}{\partial \Pi_2}\frac{\partial B}{\partial v}] + c.c. \tag{18}$$

so that the evolution of a dynamical variable A is given by

$$A_x = \{A, H\}. \tag{19}$$

In fact, Equation (11) is recovered if A is replaced by u and v in the above equation:

$$\begin{aligned} u_x = \{u, H\} = \frac{\partial H}{\partial \Pi_1} &= -i\Pi_1 \Pi_2^\star e^{-i\Delta Q x} - \Pi_{1yy}^\star \\ &= iu^\star v e^{-i\Delta Q x} + iu_{yy} \\ v_x = \{v, H\} = \frac{\partial H}{\partial \Pi_2} &= -i(\Pi_1^\star)^2 e^{+i\Delta Q x}/2 - \Pi_{2yy}^\star \\ &= iu^2 e^{+i\Delta Q x}/2 + iv_{yy}. \end{aligned} \tag{20}$$

In addition,

$$\begin{aligned} \Pi_{1x} = \{\Pi_1, H\} &= -\frac{\partial \mathcal{H}}{\partial u} \\ \Pi_{2x} = \{\Pi_2, H\} &= -\frac{\partial \mathcal{H}}{\partial v} \end{aligned} \tag{21}$$

yield the complex conjugate equations.

Equation (11) may be recast in the form of an autonomous system. For such a system, the Hamiltonian is a conserved quantity. Let $\tilde{v} = ve^{-i\Delta Q x}$, and substitute in Equation (11), resulting in

$$\begin{aligned} u_x - iK_1 u_{yy} + iu^\star \tilde{v} &= 0 \\ \tilde{v}_x - iK_2 \tilde{v}_{yy} + i\Delta Q \tilde{v} + iu^2/2 &= 0. \end{aligned} \tag{22}$$

The Hamiltonian corresponding to Equation (22) is

$$\tilde{H} = \Re[(u^\star)^2\tilde{v}] + K_1|\,u_y\,|^2 + K_2|\,\tilde{v}_y\,|^2 + \Delta Q|\,\tilde{v}\,|^2/2. \tag{23}$$

As a check:

$$\begin{aligned} u_x = \{u, \mathcal{H}\} = -\frac{\partial \mathcal{H}}{\partial u^\star} &= -iu^\star\tilde{v} + iK_1 u_{yy} \\ \tilde{v}_x = \{\tilde{v}, \mathcal{H}\} = -\frac{\partial \mathcal{H}}{\partial \tilde{v}^\star} &= -i\Delta Q\tilde{v} - iu^2/2 + iK_2 v_{yy}. \end{aligned} \tag{24}$$

Hence, the above substitution leads to a Hamiltonian with the property

$$\frac{d\mathcal{H}}{dx} = 0 \tag{25}$$

for any ΔQ.

When wavelike solutions are assumed to exist, another conserved quantity of this Hamiltonian system is

$$\frac{1}{2}(|\,u\,|^2 + |\,\tilde{v}\,|^2)_x = -\Im(K_1 u_y u^\star + K_2\tilde{v}_y\tilde{v}^\star)_y, \tag{26}$$

where $\Im$ reads as "the imaginary part of."

3 Linear Stability Analysis

The stability of the triad system to small perturbations may be inferred by slightly perturbing the system. Let

$$\begin{aligned} a_1(x,y) &= \phi(x) + \zeta(x,y) \\ a_2(x,y) &= \psi(x) + \xi(x,y), \end{aligned} \tag{27}$$

where $|\zeta|$, $|\xi|$ are both small. Further, assume $f(x,y) = f(x)$. Substituting Equation (27) into Equation (9) leads to the linear system

$$\begin{aligned} \zeta_x - iK_1\zeta_{yy} + iK_3 f(x)\zeta + iK_5 e^{-i\delta x}(\phi^\star \xi + \psi\zeta^\star) &= 0 \\ \xi_x - iK_2\xi_{yy} + iK_4 f(x)\xi + i2K_6 e^{i\delta x}\phi\zeta &= 0, \end{aligned} \tag{28}$$

with

$$\begin{aligned} \phi_x + iK_3 f(x)\phi + iK_5 e^{-i\delta x}\phi^\star\psi &= 0 \\ \psi_x + iK_4 f(x)\psi + iK_6 e^{i\delta x}\phi^2 &= 0. \end{aligned} \tag{29}$$

Separating the real and imaginary parts, let

$$\begin{aligned} \zeta &= w + it \\ \xi &= q + ir, \end{aligned} \tag{30}$$

and define

$$\begin{aligned}
\alpha_1 &= \psi_r \sin \delta x - \psi_i \cos \delta x \\
\alpha_2 &= \psi_i \sin \delta x + \psi_r \cos \delta x \\
\alpha_3 &= \phi_r \sin \delta x + \phi_i \cos \delta x \\
\alpha_4 &= \phi_i \sin \delta x - \phi_r \cos \delta x, \qquad (31)
\end{aligned}$$

where the subscripts r and i refer to the real and imaginary part, respectively, of the quantity.

If we substitute Equation (30) and Equation (31) into Equation (28), the system is now

$$\mathbf{u}_x - \mathbf{A} \cdot \partial_{yy}\mathbf{u} + \mathbf{B} \cdot f(x)\mathbf{u} + \mathbf{C} \cdot \mathbf{u} = 0, \qquad (32)$$

with $\mathbf{u} = [w, t, q, r]^T$ and the matrices

$$\mathbf{A} = \begin{pmatrix} 0 & -K_1 & 0 & 0 \\ K_1 & 0 & 0 & 0 \\ 0 & 0 & 0 & -K_2 \\ 0 & 0 & K_2 & 0 \end{pmatrix}, \qquad (33)$$

$$\mathbf{B} = \begin{pmatrix} 0 & -K_3 & 0 & 0 \\ K_3 & 0 & 0 & 0 \\ 0 & 0 & 0 & -K_4 \\ 0 & 0 & K_4 & 0 \end{pmatrix}, \qquad (34)$$

which are constant, and

$$\mathbf{C} = \begin{pmatrix} K_5\alpha_1 & K_5\alpha_2 & K_5\alpha_3 & K_5\alpha_4 \\ K_5\alpha_2 & -K_5\alpha_1 & -K_5\alpha_4 & K_5\alpha_3 \\ 2K_6\alpha_3 & 2K_6\alpha_4 & 0 & 0 \\ -2K_6\alpha_4 & -2K_6\alpha_3 & 0 & 0 \end{pmatrix}, \tag{35}$$

which is a function of x. Assume a separable solution, that is, $\mathbf{u} = \mathbf{X}(x)\mathbf{Y}(y)$. Thus,

$$\mathbf{u} = \mathbf{U}e^{\pm i\mathbf{\Lambda}y}\exp[-\mathbf{A}\cdot\mathbf{\Lambda}x]\exp[-\mathbf{B}\int^x f(s)ds - \int^x \mathbf{C}(s)ds]. \tag{36}$$

The vector $\mathbf{U}$ is constant whose value depends on the conditions at $x = 0$. It is helpful in what follows to look at this solution in component form:

$$\begin{aligned} w &= U_1 e^{\pm\Lambda_1 y}\exp[K_1\Lambda_2^2 x]\exp[K_3\int^x f(s)ds - \int^x C_1(s)ds] \\ t &= U_2 e^{\pm\Lambda_2 y}\exp[-K_1\Lambda_1^2 x]\exp[-K_3\int^x f(s)ds - \int^x C_2(s)ds] \\ q &= U_3 e^{\pm\Lambda_3 y}\exp[K_2\Lambda_4^2 x]\exp[K_4\int^x f(s)ds - \int^x C_3(s)ds] \\ r &= U_4 e^{\pm\Lambda_4 y}\exp[-K_2\Lambda_3^2 x]\exp[-K_4\int^x f(s)ds - \int^x C_4(s)ds]. \end{aligned} \tag{37}$$

It is apparent from these expressions that growth and decay from spanwise perturbations of the real part of the modes depend on the spectrum of their imaginary counterparts, and vice versa. In the most general case the solutions will become unstable if any one of the following conditions is met:

$$-\nu_1 y + K_1(\mu_2^2 - \nu_2^2)x + K_3\int^x f(s)ds - \int^x C_1(s)ds \;>\; 0$$

$$
\begin{aligned}
-\nu_2 y + K_1(\mu_1^2 - \nu_1^2)x - K_3 \int^x f(s)ds - \int^x C_2(s)ds &> 0 \\
-\nu_3 y + K_2(\mu_4^2 - \nu_4^2)x + K_4 \int^x f(s)ds - \int^x C_3(s)ds &> 0 \\
-\nu_4 y + K_2(\mu_3^2 - \nu_3^2)x - K_4 \int^x f(s)ds - \int^x C_4(s)ds &> 0,
\end{aligned} \tag{38}
$$

where $\Lambda_j = \mu_j + i\nu_j$. Typically the system is prepared in such a way that $t(x = 0, y) = 0$ and $r(x = 0, y) = 0$. When Λ_j are purely real, the onset of instability occurs when either

$$
\begin{aligned}
K_3 \int^x f(s)ds - \int^x C_1(s)ds &> 0, \text{ or} \\
K_4 \int^x f(s)ds - \int^x C_3(s)ds &> 0.
\end{aligned} \tag{39}
$$

Plots of C_1 and C_3 for $f(x) = 0$, $\mathcal{A}_1 = 0.5$, $\mathcal{A}_2 = 0.01$, and with parameters $\alpha = 0.1$, $\beta = 0.1$, and $\omega_1 = 1.2$ are shown in Figures 5 and 6.

4 An Exactly-Solvable Case

When the bottom is flat and the boundary conditions are constant, the triad system becomes

$$
\begin{aligned}
a_{1x} + iK_5 e^{-i\delta_x} a_1^\star a_2 &= 0 \\
a_{2x} + iK_6 e^{+i\delta_x} a_1^2 &= 0 \\
a_1(x = 0, y) &= \mathcal{A}_1 \\
a_2(x = 0, y) &= \mathcal{A}_2,
\end{aligned} \tag{40}
$$

where $\mathcal{A}_j$ are constants. The above system is familiar to the nonlinear optics community; cf. [4]. In what follows we adapt some of the results of Brekhovskikh

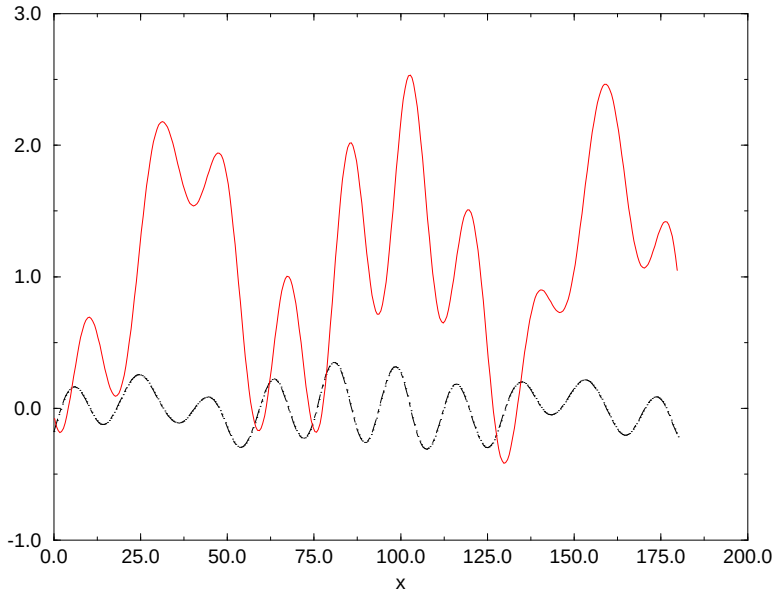

Figure 5: Typical values of C_1, dashed line, and $\int^x C_1(s)ds$, versus x, for a flat bottom.

and Goncharov [5] to the problem at hand.

Letting $a_i = A_i(x)\exp\theta_i(x)$ in Equation (40), and replacing

$$X = A_2 \sin\Omega \tag{41}$$

$$Y = A_2 \cos\Omega \tag{42}$$

$$Z = A_1^2, \tag{43}$$

with $\Omega = 2\theta_1 - \theta_2 + \delta x$, we obtain the statement of conservation of energy

$$K_5(X^2 + Y^2) + K_6 Z = E_0, \tag{44}$$

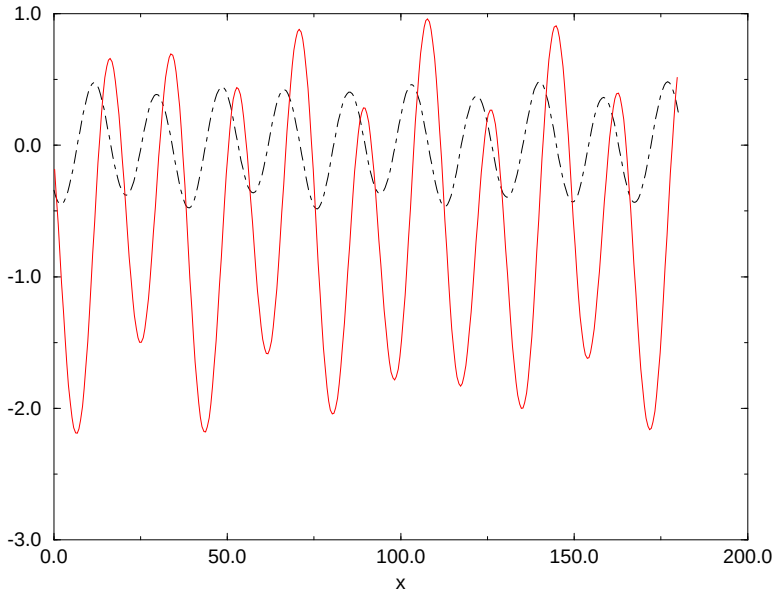

Figure 6: Typical values of C_3, dashed line, and $\int^x C_3(s)ds$, versus x, for a flat bottom.

and the equation

$$\frac{dX}{dY} = \frac{K_5(X^2 + 3Y^2) - \delta Y - E_0}{(\delta - 2K_5 Y)X}, \tag{45}$$

which may be used to investigate the structure of the phase plane of A_2. The dynamics of A_1 follow immediately from the conservation of the energy constraint, Equation (44). Three cases, depending on the size of the detuning parameter δ, are investigated. A plot of the detuning parameter as a function of frequency and β is shown in Figure 7 for the dispersion relation given by

$$\omega^2 - \frac{k^2}{1 + \frac{1}{3}\beta^2 k^2} = 0, \tag{46}$$

where $k_2 = 2k_1 - \delta$, and $\omega_2 = 2\omega_1$. When $\delta/2\sqrt{E_0} \sim 0$, the phase plane is shown in Figure 8. Note that $dX/dY = 0$ and $X = 0$ give the two centers,

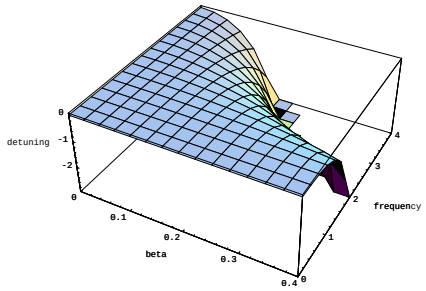

Figure 7: Detuning parameter dependence on ω_1 and β for the water wave problem.

at $(X, Y) = (0, \pm\sqrt{E_0}/\sqrt{3K_5})$. Setting $Y = 0$, $dX/dY = 0$ gives the radius of the bounding circle, at $\sqrt{E_0}/\sqrt{K_5}$, beyond which the orbits diverge. Additionally, there are two saddle points at $(X, Y) = (\pm\sqrt{E_0}/\sqrt{K_5}, 0)$. Motion along the limiting circle takes place in such a way that $A_1 = 0$ and $A_2 = E_0/\sqrt{K_5}$. If, for example, $A_1 \neq 0$ and $A_2 = 0$ initially, motion in the plane takes place along the line $Y = 0$ up to the limiting curve, the phase Ω is then equal to $\pi/2$. From the imaginary part of the original system, it may be deduced that the variation of Ω in this limit is described by

$$\Omega_x - 2K_5 E_0^{1/2} \cos\Omega = 0. \tag{47}$$

The transition from the state $\sin\Omega = 1$ to $\sin\Omega = -1$ occurs along the limiting circle. The distance x at which this transition occurs is infinite, but it can be estimated by solving Equation (47). The solution is

$$\Omega = \tan^{-1}[\exp(-2K_5 E_0^{1/2} x)\tan\Omega_0], \tag{48}$$

and hence an estimate of the spatial length at which the energy of the first mode

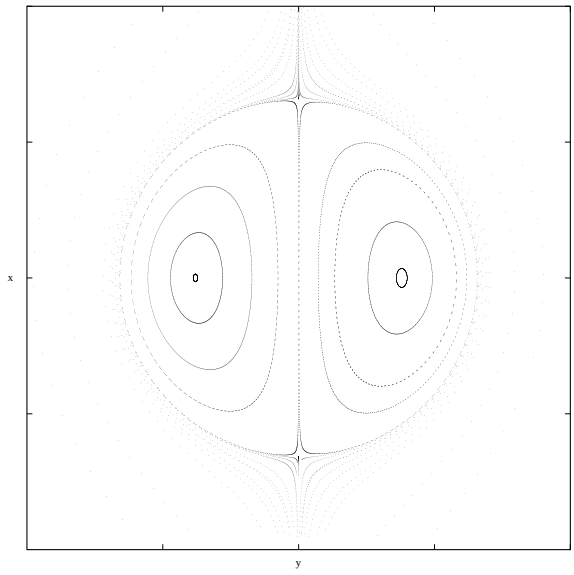

Figure 8: Phase plane for A_2 for $\delta \sim 0$. X axis is vertical.

makes an almost complete transition to the second mode is

$$L \approx 1/2K_5E_0^{1/2}, \tag{49}$$

which subsequently will be seen as related to the "interaction length." The variation of the amplitude of A_2 along $Y = 0$ may be discerned from

$$A_{2x} = K_5A_2^2 - E_0, \tag{50}$$

which is obtained by eliminating Z from Equation (40) and making use of the energy relationship.

The solution of Equation (50) is

$$A_2 = (E_0/K_5)^{1/2} \tanh[K_5^{1/2}E_0^{1/2}(x - x_0)], \tag{51}$$

with $\mathcal{A}_2 = (E_0/K_5)^{1/2}\tanh[(K_5E_0)^{1/2}x_0]$. At the beginning of the growth process, $A_1 \gg A_2$ so that $\sin\Omega = 1$ and the growth of the second mode is independent of $\mathcal{A}_2$. With the solution of A_2 in hand, using Equations (44) and the first expression of Equation (40), we can show that

$$A_1(x) = \frac{\mathcal{A}_1}{\sqrt{1-\tanh^2[K_5^{1/2}E_0^{1/2}x_0]}} sech\sqrt{K_5E_0}(x-x_0). \tag{52}$$

From this solution we conclude that irreversible energy conversion takes place for $\delta = 0$. This solution is not stable, however, since the stationary states are reached by motion along the limiting curve on the phase plane. The smallest of δ invariably results in motion along homoclinic orbits with consequent oscillations in the amplitude of A_1 and A_2.

For the case $\delta \neq 0$, but small compared to $2E_0^{1/2}$, the curves have similar structure to the case previously discussed. The phase is described by

$$\Omega_x + \delta - 2K_5E_0^{1/2}\cos\Omega = 0. \tag{53}$$

Consequently, the interaction length is decreased:

$$L = \frac{1}{\sqrt{4K_5E_0^{1/2} - \delta^2}}. \tag{54}$$

With regard to the sand ridge model, the interaction length is correlated to the inter-bar spacing. From Equation (53) it is seen that the bar spacing will decrease for higher frequencies in the water waves.

The centers are now at $(X,Y) = (0, \frac{\delta}{6K_5}[1 \pm \sqrt{1+\frac{12K_5E_0}{\delta^2}}])$, and the line $Y = 0$

is no longer the line of symmetry. Also, the line $Y = \frac{\delta}{6K_5}$ does not generally intersect the limiting circle, as can be seen in Figure 9. Instead of two pairs of

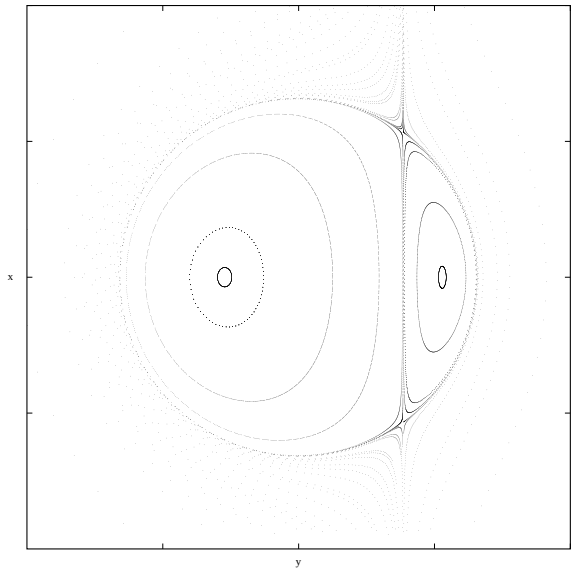

Figure 9: Phase plane for A_2 for $\delta/2E_0^{1/2} \ll 1$. X axis is vertical.

stationary solutions, only one is possible, and the energy is concentrated mainly in the lower mode. The two modes interact weakly, and the spatial beats get smaller and shallower as the detuning paramenter is increased. In fact, when $\delta/2E_0^{1/2} \gg 1$, $A_1(x) \sim \mathcal{A}_1$, and $A_2(0) = \mathcal{A}_2$, the first two terms in Equation (53) are dominant, so that the phase is

$$\Omega = \delta x + \pi/2. \tag{55}$$

Substituting the above expression into the second expression of Equation (40), we can show that

$$A_2 = \mathcal{A}_2 + \frac{K_6}{\delta}\mathcal{A}_1^2 \sin \delta x. \tag{56}$$

The phase portrait for this case is shown in Figure 10.

Figure 10: Phase plane for A_2 for $\delta/2E_0^{1/2} \gg 1$. X axis is vertical.

We remark that of the three cases considered here, only the first two are physically relevant to the sand ridge generation problem. The large detuning parameter case violates assumptions on the size of the wavenumber/frequency in the model. Much is to be learned about the triad system, however, from looking at the high-frequency case in some detail.

When ω_1 is large (or, equivalently, when δ is large), the amount of energy from the first mode transferred to the second one may be quite small. As was just mentioned, in this case the first mode has nearly constant amplitude. Assume that the boundary conditions are constant, i.e. $a_j(0) = \mathcal{A}_j$. Thus, $a_1(x) \sim \mathcal{A}_1$, and the second mode expression of Equation (40) may be integrated, yielding

$$a_2(x) = \frac{K_6}{\delta}\mathcal{A}_1^2 e^{\delta x}. \tag{57}$$

Substituting Equation (57) into the first mode equation, we get

$$a_{1x}(x) \approx \frac{iK_5}{\delta} a_1 |\mathcal{A}_1^2| e^{-\delta x}, \tag{58}$$

which can readily be integrated to yield

$$a_1(x) = \mathcal{A}_1 e^{\sigma x}, \tag{59}$$

where $\sigma = K_5 K_6 / \delta |\mathcal{A}_1^2|$. Thus, $a_1(x)$ is approximately sinusoidal, with a wavelength proportional to $|\mathcal{A}_1^2|$.

For a nonflat bottom, which is typical of the bottom topography in the ocean setting, an exact solution is not possible. Consider, however, the case

$$\begin{aligned} A_{1x} - K_5 A_1 A_2 \sin\Omega + \chi_1 A_1 &= 0 \\ A_{2x} + K_6 A_1^2 \sin\Omega + \chi_2 A_2 &= 0, \end{aligned} \tag{60}$$

where χ_j represent constants. An analytical solution of this system is not possible, unless $\chi_1 = \chi_2 = \chi$, in which case, conservation of energy is given by

$$K_5 A_1^2 + K_6 A_2^2 = E_0 e^{-2\chi x}. \tag{61}$$

Introducing new variables

$$\begin{aligned} X &= \tilde{X} E_0^{1/2} e^{-\chi x} \\ Y &= \tilde{Y} E_0^{1/2} e^{-\chi x} \end{aligned} \tag{62}$$

and the reduced distance

$$\xi = 2E_0^{1/2}(1 - e^{-\chi x})/\chi, \tag{63}$$

assuming $\delta = 0$, we obtain, using Equation (61) the system's phase plane equation

$$2\frac{d\tilde{X}}{d\tilde{Y}} = \frac{1 - \tilde{X}^2 - 3\tilde{Y}^2}{\tilde{X}\tilde{Y}}, \tag{64}$$

which has the same structure in the phase plane as that shown in Figure 8. The important distinction is that ξ is related nonlinearly to x. Thus, the damping of the waves is characterized by

$$\tilde{\chi} = \chi/(2K_5 E_0^{1/2}). \tag{65}$$

For $\tilde{\chi} \ll 1$, there is weak damping, and the waves travel a considerable distance before the energy is fully dissipated. On the other hand, if $\tilde{\chi} \gg 1$, only a small arc of the trajectory in phase plane is traversed. The wave substantially attenuates in a short distance. The relevant case, at least approximately, to the oceanic problem is the former case, in which the size of the bottom makes the coefficient analogous to χ in the above presentation of $O(\alpha)$ in size relative to the other terms in Equation (60). We can infer from this result that milder average slopes in the bottom topography favor the formation of sand ridge fields with many bars and that the separation between the bars becomes shorter as the waves shoal.

The solution for small ΔQ and large ΔQ is graphically depicted in Figure 11. In

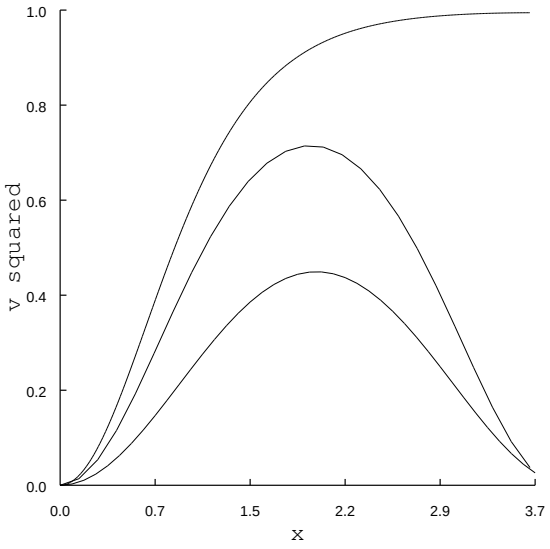

Figure 11: $|a_2|^2$ dependence on the detuning parameter. In all cases $|a_1|^2(x = 0) = 1$. The interaction length and the power transferred to $|a_2|^2$ decreases as ΔQ increases.

the first case, the interaction length is relatively insensitive to ΔQ and substantial power transfer occurs, the interaction length is very large. On the other hand, for $\Delta Q \gg 1$, there is less power transfer and the interaction length is shorter. Figure 12 shows how the interaction length varies nonlinearly with ΔQ. Figures 13 and 14 illustrate the dependence of the interaction length on the size of the nonlinear parameter α and the dispersion parameter β. The relevant size of the parameters α and β in the sand ridge case is as high as 0.15 for α and $0.005 < \beta < 0.15$. Hence, from the graphs it may be inferred that the interaction length is more sensitive to dispersion than to nonlinearity for the above-mentioned ranges of α and β.

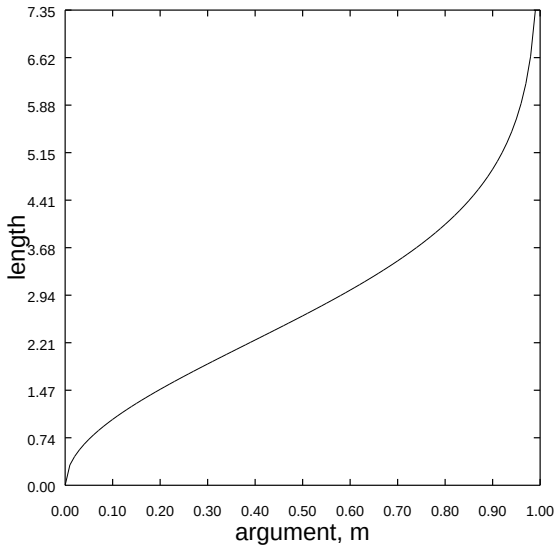

Figure 12: Interaction length dependence on the nonlinear parameter ΔQ. The detuning parameter is scaled so that as $\Delta Q \to 0$, $m \to 1$.

5 High-Frequency Behavior

As a way to assess the evolution of waves with periodicity in the longshore direction, suppose

$$\begin{aligned} a_1(x,y) &= u(x,y)e^{i(k_1 x - \omega_1 t + l_1 y)} \\ a_2(x,y) &= v(x,y)e^{i(k_2 x - \omega_2 t + l_2 y)} \end{aligned} \tag{66}$$

Then the system (9) is now

$$u_x + il_1^2 K_1 u + iK_5 u^\star v e^{-i(\gamma y + \delta x)} = 0 \tag{67}$$

$$v_x + il_2^2 K_2 v + iK_6 u^2 e^{+i(\gamma y + \delta x)} = 0, \tag{68}$$

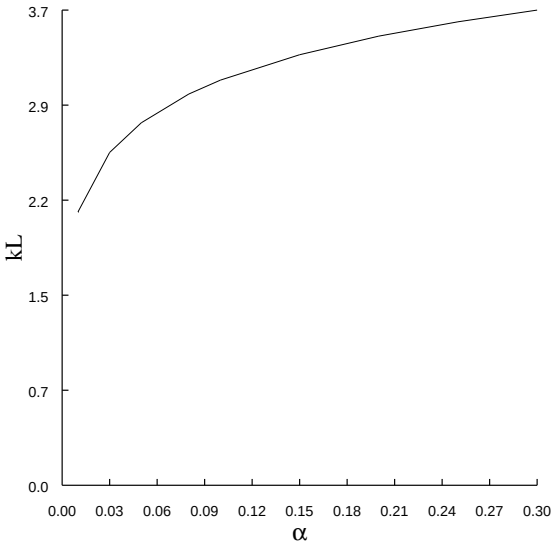

Figure 13: Interaction length dependence on the nonlinear parameter α.

where $\gamma = l_2 - 2l_1$, which can be zero. We now consider the high-frequency case. For ω_1 large, $u(x,y) \sim u^0$. Hence Equation (68) may be integrated, yielding

$$v = -\frac{K_6 u^2 e^{i(\gamma y + \delta x)}}{\delta + l_2^2 K_2}, \tag{69}$$

assuming $v(x=0,y) = 0$ and $u(x=0,y) = u^0$ constant. Using this expression in Equation (67), we have

$$u(x,y) = u^0 \exp[-il_1^2 K_1 x + i\frac{K_5 K_6 |\, u^0 \,|^2 x}{\delta + l_2^2}]. \tag{70}$$

Hence v oscillates with lines of constant phase normal to the $\tan^{-1}(\frac{\gamma}{\delta})$ direction, where the angle is taken with respect to the shoreward direction. When $l_2 = 2l_1$ exactly, the direction of constant phase orthogonals is the shoreward direction. On

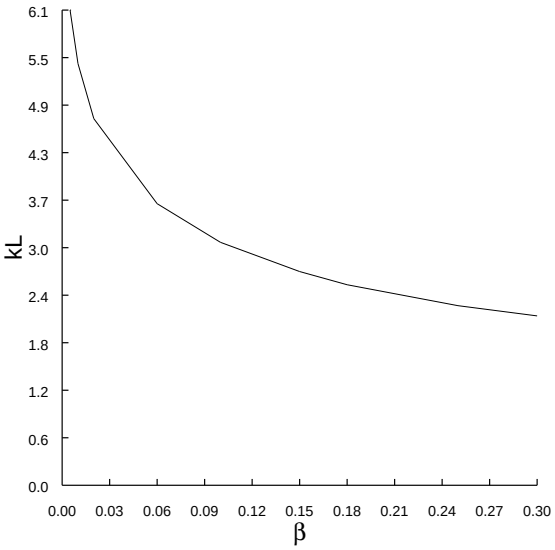

Figure 14: Interaction length dependence on the dispersion parameter β.

the other hand, u oscillates in the x direction, with a repetition length

$$L_\gamma = \frac{\delta + l_2^2 K_2}{2\pi}\{K_5 K_6 |\, u^0\,|^2 - (\delta + l_2^2 K_2) l_1^2 K_1\}^{-1}. \tag{71}$$

Furthermore, v can develop a singularity when

$$\delta + l_2^2 K_2 = 0, \tag{72}$$

that is, when $l_2 = \pm\sqrt{-\delta/K_2}$ (note that $\delta \leq 0$). In terms of the y component of the wavenumber, the singularity occurs when

$$l_2 = \pm\sqrt{\frac{-2\delta k_2}{\alpha}}. \tag{73}$$

An l_2 of such value is not at all unreasonable to consider. There is a change in sign in v on either side of the location at which the singularity is predicted.

Yet another interesting feature is the situation when

$$|u^0|^2 = (\delta + l_2^2 K_2) l_1^2 K_1 / K_5 K_6, \tag{74}$$

again, a reasonable value. In such an event, the modulation of u practically disappears. Then

$$u(x,y) \approx u^0 = \pm\sqrt{(\delta + l_2^2 K_2) l_1^2 K_1 / K_5 K_6} \tag{75}$$

and

$$v(x,y) = -\frac{l_1^2 K_1 e^{i(\delta x + \gamma y)}}{K_5}, \tag{76}$$

which is a simple sine wave. Hence, one could conceivably use modulations in the y direction to nonlinearly produce linear sine wave signals of the second harmonic with amplitude given by l_1^2. If $l_2 = 2l_1$ exactly, the wave oscillates in the shoreward direction.

Carrying out this high-frequency analysis further, we can consider the effect of the bottom topography under special circumstances: the case when $f(x,y) = f(y)$ leads in a straightforward manner to

$$v = -\frac{K_6 u^2 e^{i(\gamma y + \delta x)}}{\delta + l_2^2 K_2 + K_4 f(y)}, \tag{77}$$

again assuming $v(x=0,y)=0$ and $u(x=0,y)=u^0$ constant, and

$$u(x,y)=u^0\exp[-il_1^2K_1x+i\frac{K_5K_6|\,u^0\,|^2x}{\delta+K_2l_2^2+K_4f(y)}]. \tag{78}$$

Thus, the effect of the bottom in this case is to change the amplitude of v and, at the same time, modulate the oscillations of u. Again, the possibility of a singularity and a change in sign in v exists.

Finally, the same method may be employed to assess the effect of a mildly sloping bottom on the high-frequency solution. Assume $f(x,y)=\nu x/2$, where ν is small. The same procedure leads to

$$\begin{aligned} v &\approx -\frac{(u^0)^2K_6e^{i(\gamma y+\delta x)}}{\delta+K_2l_2^2} \\ &\quad [1-i\frac{2K_4\nu}{(\delta+K_2l_2^2)^2}\{(\delta+K_2l_2^2)^2x^2/2+i(\delta+K_2l_2^2)x-1\}]e^{-iK_4\nu x^2} \\ u &\approx u^0\exp\{-i(K_1l_1^2 \\ &\quad -\frac{|\,u^0\,|^2K_5K_6}{(\delta+K_2l_2^2)^2})x-i(K_3-\frac{|\,u^0\,|^2K_4K_5K_6}{(\delta+K_2l_2^2)^2})\nu x^2\} \\ &\quad \exp-\frac{2|\,u^0\,|^2K_4K_5K_6\nu}{(\delta+K_2l_2^2)^3}(x-\frac{(\delta+K_2l_2^2)^2x^2}{2}). \end{aligned} \tag{79}$$

The result is valid only for $K_4\nu x^2\ll 1$. That is, since K_4 is of the same order as $k_2\varepsilon$, it is valid for $x\ll O(1/\sqrt{k_2\varepsilon\nu})$. To discern what is fundamentally different about the sloping case, consider the situation in which u^0 has no y dependence, so that Equation (79) has the form

$$v \approx -\frac{(u^0)^2K_6e^{i\delta x}}{\delta}$$

$$
\begin{aligned}
& [1 - i\frac{2K_4\nu}{\delta^2}(\frac{\delta^2 x^2}{2} - i\delta x - 1)]e^{-iK_4\nu x^2} \\
u \approx\ & u^0 \exp\{i\,|u^0|^2 K_5 K_6 x/\delta - i(K_3 - \frac{|u^0|^2 K_4 K_5 K_6}{\delta^2})\nu x^2\} \\
& e^{\frac{-2|u^0|^2 K_4 K_5 K_6 \nu}{\delta^3}(x - \delta^2 x^2/2)}.
\end{aligned}
\tag{80}
$$

From Equation (80) it is readily apparent that v oscillates proportionally to $e^{i\delta x}$, its maximum amplitude δ/K_6 times smaller than u^2. The phase will drift quadratically with distance and proportionally to $K_4\nu$. The amplitude drops linearly at a rate proportional to the size of $K_4\nu$ and $K_3\nu$; the wave decays exponentially at a rate controlled by the last exponential in the above expression. To properly interpret the decay, recall that $|\delta| \gg 1$ and δ is strictly negative in this analysis. The second term in the exponential implies that decay/blow up would be a possible outcome of the original model. However, this is an artifice of the present analysis. If the assumption $u(x) \sim$ constant is violated, the above expressions are not valid. Thus, for our interpretation to be valid, it is required that $2|u|^2 K_4 K_5 K_6 \nu x/\delta^3 \ll 1$.

A very important question that arises in the applicability of slightly resonant interacting triad expansion techniques to oceanic waves is that we may be neglecting very important side-band modulations. These can be producing interesting structure, controlling the stability of the primary waves, or affecting very minimally the structure of the evolving waves. A general result on this issue is forthcoming, but for now we limit our attention to the high-frequency case. The problem of bands, rather than isolated modes, and the effect on the evolution of individual waves has been examined by Hasselmann [6] in the context of deep oceanic waves. Appli-

cable to the shallow water case considered here, Brekhovskikh and Goncharov [5] examined this issue, and in what follows their findings are paraphrased.

First, the modal expansion is replaced by the more familiar expression for the lowest-order velocity

$$u_0(x,t) = \int_{-\infty}^{\infty} a_\omega(x) e^{-i\omega t} d\omega, \tag{81}$$

where $a_\omega(x) \equiv a(x\omega)$, and $a^\star_\omega(x) = a_{-\omega}(x)$ since u_0 is real. Assume $a_\omega = \rho_\omega \exp(ik_\omega x)$, where $k_\omega = k(\omega)$ is found by the dispersion relation. Again, reality means that $k^\star_\omega = k_{-\omega}$ and $\rho^\star_\omega = \rho_{-\omega}$. Substituting Equation (81) into the original equations and using the compatibility conditions, we obtain an expression for the amplitude of the incident waves:

$$\frac{\partial}{\partial x}\rho_\omega = -i\alpha\omega \int_{-\infty}^{\infty} \rho_q \rho_s \exp(-i\Delta_{qs\omega} x) dq, \tag{82}$$

where $s = \omega - q$ and $\Delta_{qs\omega} = q + s - k_\omega$. If the incoming harmonic wave $u(0,t) = a_1(0)e^{-i\omega_1 t} + c.c.$ (i.e., $\rho_\omega(0) = a_1(0)\delta(\omega - \omega_1) + a^\star_1(0)\delta(\omega + \omega_1)$), the spectrum of $u(x,t)$ remains discrete at any time; the only nonzero components are $\omega_n = n\omega_1$, $k_n = k(\omega_n), n = \pm 1, \pm 2, \cdots$, and

$$a_\omega(x) = \sum_n a_n(x)\delta(\omega - \omega_n). \tag{83}$$

Then Equation (82) yields

$$\frac{\partial}{\partial x} a_n = -i\alpha\omega_n \sum_m a_m a_l e^{-i\Delta_{mln} x}, \tag{84}$$

$l = n - m$, $\Delta_{mln} = k_m + k_l - k_n$, $a_n = a_n^\star$, and $a_0 = 0$.

Taking ω_1 as the principal harmonic and $\delta\omega$ as the width of the spectral band, we extend Equation (40) to include the interactions of spectral components of the wave train with long-wavelength waves. Except for a constant multiplying the integral, the spectral amplitude equation is

$$\begin{aligned}
\frac{\partial}{\partial x}\rho(\omega) &= -i\alpha\omega \int_{\Delta\omega} [\rho_{\omega_1+\xi}\rho_{\omega-\omega_1-\xi}e^{i\Delta_+ x} + \rho_{-\omega_1+\xi}\rho_{\omega+\omega_1+\xi}e^{i\Delta_- x}]d\xi, \\
\Delta_\pm &= k_\omega \mp k_{\omega_1+\xi} \pm k_{\omega_1+\xi\mp\omega} \approx k_\omega \mp k_{\omega_1} \pm \frac{dk}{d\omega}|_{\omega_1}\xi, \\
\pm k_{\omega_1} \pm \frac{dk}{d\omega}|_{\omega_1}(\xi - \omega) &= k_\omega - c_g^{-1}\omega = [c_{ph}^{-1}(0) - c_g^{-1}]\omega = \Delta\omega, \qquad (85)
\end{aligned}$$

where c_g is the group velocity and c_{ph} is the phase velocity. Approximating, we have

$$\begin{aligned}
\rho_{\omega_1+\xi} &\approx \rho_{\omega_1+\omega+\xi} \approx \rho_{\omega_1}, \\
\rho_{-\omega_1+\omega+\xi} &\approx \rho_{-\omega_1+\xi} \approx \rho_{-\omega_1}, \qquad (86)
\end{aligned}$$

and the equation for the amplitude is

$$\frac{\partial}{\partial x}\rho_\omega \approx -i\alpha\omega|\rho_{\omega_1}|^2 e^{i\Delta\omega x}\Delta\omega. \qquad (87)$$

As was done in the discrete case, assume the frequency is sufficiently high so that $\rho_{\omega_1} \approx$ constant. Thus,

$$\rho_\omega(x) \approx -\alpha\frac{\omega}{\Delta\omega}|\rho_{\omega_1}|^2 e^{i\Delta\omega x}\Delta\omega = -\frac{\alpha|\rho_{\omega_1}|^2 e^{i\Delta\omega x}\Delta\omega}{[c_{ph}^{-1}(0) - c_g^{-1}(\omega_1)]}. \qquad (88)$$

The following equation for ρ_ω corresponds to such an interaction:

$$\rho_\omega = -i\alpha\omega \int_{\Delta\omega} \rho_\xi \rho_{\omega-\xi} e^{-i\Delta_\xi x} d\xi \approx \frac{i\alpha^2\omega_1 |\rho_{\omega_1}|^2 \rho_\omega (\Delta\omega)^2}{[c_{ph}^{-1}(0) - c_g^{-1}(\omega_1)]}, \tag{89}$$

where $|\omega - \omega_1| \leq \Delta_\omega$. Let $a_1 = \rho_\omega \Delta_\omega$ stand for the amplitude of the principal harmonic. Then, taking into account the term corresponding to the interactions with the second harmonic, we obtain, instead of Equation (58),

$$\frac{\partial}{\partial x} a_1 = i\alpha^2\omega^2 |a_1|^2 \{\Delta^{-1} + \omega^{-1}[c_{ph}^{-1}(0) - c_g^{-1}(\omega_1)]^{-1}\} a_1. \tag{90}$$

Its solution is $a_1 = a_1(0)e^{i\sigma x}$, corresponding to waves with "spatial" shift of $\sigma = -\alpha^2\omega^2 |a_1|^2 \{\Delta^{-1} + \omega^{-1}[c_{ph}^{-1}(0) - c_g^{-1}(\omega_1)]^{-1}\}$. Hence, in the high frequency the main difference between the discrete and the banded spectrum case is that the latter has an additional term in the nonlinear shift as compared with the case of Equation (58).

The conditions for the stability of the triad system and of the full model, as of this writing, have not been analyzed in detail. However, it is possible to infer from the results of this section that the stability of the triad system does not depend on the frequency of the water waves since only weak resonance is possible, which in turn means that less energy is shifted from the lower modes to the higher ones the higher the frequency of the fundamental mode.

6 Conclusions and Suggestions for Further Research

The triad system that forms part of a model for the formation and evolution of sand ridges is rich in mathematical structure. It is clear from our results that we have only begun to understand the full meaning of the system.

The high-frequency regime of the system has been considered in greater detail here because results from similar problems, primarily by the nonlinear optics community, were easily adaptable to our case. The low-frequency regime, which is more relevant to the sand ridge problem, was considered only in cursory fashion. Hence, future work will be aimed at gaining a better understanding of the system in the low-frequency regime.

Several issues require our immediate attention. First, we need to further our understanding of the refractive behavior of the waves under the action of a fully featured bottom. As shown in [1] and [2], there are a number of ways in which refraction occurs in the surface waves. The model's assumptions place a restriction on the degree of spanwise dependence of the solutions, and care must be exercised so as to not violate the assumption, especially when the domain involved is large. It may be possible, however, even when weak y dependence assumptions are not violated, for the solutions to lose their stability as a result of severe refraction. At a later stage in this study we shall pursue this issue, with the hopes of arriving at an estimate of when and how this form of instability occurs. Second, a comprehensive stability analysis is needed. Evidence from numerical calculations and of our preliminary analytical work on the subject suggests that the stability is

controlled by the possibility of a singularity in the denominators of the coefficients K_5 and K_6, by the right combination of parameters (see Figures 15 and 16) or by the choice of boundary conditions $\mathcal{A}_i$. Third, we need to prove the existence and uniqueness of solutions of the system. Fourth, we need to study properties related to the system's Hamiltonian structure. In our preliminary work we found no evidence of complete integrability. And fifth, we need a thorough study of the issue of resonance between the surface waves and the bottom topography.

Regarding the full sand ridge model, the most interesting issue is the study of steady state bottom configurations. Preliminary results exist for the two-dimensional case [7]; however, this case is far from fully explored. The three-dimensional case has received no attention.

Further developments on the sand ridge model are planned. In particular, work is under way to couple the mass transport equation to a full Boussinesq system, the aim being to consider more realistic water wave spectra as agents of order for the bottom topography. Additionally, we plan to consider a mass transport model that enables the inclusion of shear stresses.

On the experimental side, work is under way to compare the model presented in this series of papers with field data gathered in Eastern Australia and off the coast of Newfoundland.

Acknowledgments

We thank the Applied Research Laboratory at The Pennsylvania State University for making this project possible. This work was also supported by the Office of Scientific Computing, U.S. Department of Energy, under Contract W-31-109-Eng-38.

A Appendix

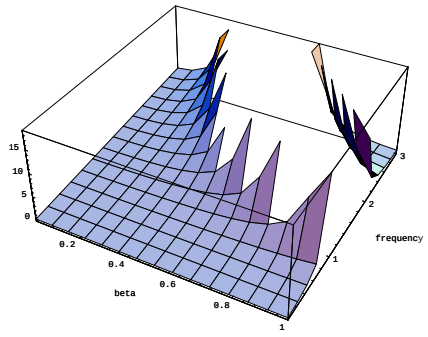

Figure 15: Plot of K_5/α versus the fundamental frequency ω_1, and β for the water wave problem.

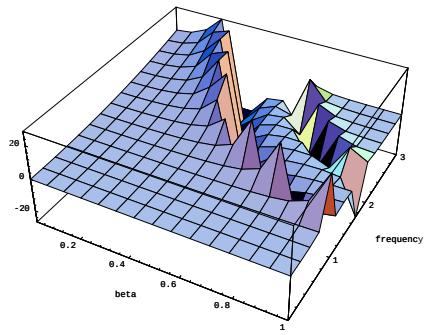

Figure 16: Plot of K_6/α versus the fundamental frequency ω_1, and β for the water wave problem.

The following are constants associated with Equation (8):

$$K_1 = F_1$$

$$K_2 = F_2$$

$$\begin{aligned} K_3 &= D_1 E_1 \\ K_4 &= D_2 E_2 \\ K_5 &= D_1 S_1 \\ K_6 &= D_2 S_2 \end{aligned} \tag{91}$$

with

$$\begin{aligned} D_j &= [2(1-\beta^2\tfrac{\omega_j^2}{3})]^{-1} \\ E_j &= k_j(1-\tfrac{2}{3}\beta^2\omega_j^2) \\ F_j &= 1/2k_j \\ S_1 &= \tfrac{k_2-k_1}{\omega_1}\{k_2-k_1+\omega_1(\tfrac{\omega_1}{k_1}+\tfrac{\omega_2}{k_2})\} \\ S_2 &= 2(k_1^2/+2\omega_1^2)/\omega_2. \end{aligned} \tag{92}$$

The constants K_5 and K_6 are illustrated in Figures 15 and 16, respectively.

References

[1] J. M. Restrepo & J. L. Bona, "Model for the Formation of Longshore Sand Ridges on the Continental Shelf," Mathematics and Computer Science Division, Argonne, Ill, December 1993.

[2] J. M. Restrepo & J. L. Bona, "Model for the Formation of Longshore Sand Ridges on the Continental Shelf: The Interaction of Internal Waves and the Bottom Topography," Mathematics and Computer Science Division, Argonne, Ill, December 1993.

[3] J. M. Restrepo & J. L. Bona, "Discretization of a Model for the Formation of Longshore Sand Ridges," Mathematics and Computer Science Division, Argonne, Ill, December 1993.

[4] J. A. Armstrong, J. Ducuing & P. S. Persham, "Interaction between Light Waves in a Nonlinear Dielectric," *Physical Review* 127 (1962), 1918–1939.

[5] L. M. Brekhovskikh & V. Goncharov, *Mechanics of Continua and Wave Dynamics*, Springer Series on Wave Phenomena #1, Springer-Verlag, New York, 1985.

[6] K. Hasselmann, "On the Nonlinear Energy Transfer in a Gravity-Wave Spectrum," *Journal of Fluid Mechanics* 12 (1962), 481–500.

[7] B. Boczar-Karakiewicz, J. L. Bona & G. Cohen, *Interaction of Shallow-water waves and bottom topography*, PSU Applied Mathematics Series #AM3, Penn State University, 1986.

List of Figures

1 $a_1(x,y)$ for $\mathcal{A}_1 = 0.5 + 0.1\sin(\frac{3}{N}\pi y)$, $\mathcal{A}_2 = 0$, and $\delta \neq 0$. 7

2 $a_1(x,y)$ for $\mathcal{A}_1 = 0.1\sin(\frac{3}{N}\pi y)$, $\mathcal{A}_2 = 0$, and $\delta \neq 0$. 8

3 $a_1(x,y)$ for boundary conditions $\mathcal{A}_1 = 0.1\sin(\frac{3}{N}\pi y)$, $\mathcal{A}_2 = 0$, and detuning parameter $\delta = 0$. 9

4 Solution for quasi-periodic boundary conditions: $\mathcal{A}_1 = 0.1[\sin(\frac{3}{N}\pi y) + \sin(\frac{8}{N}\pi y)]$, and $\mathcal{A}_2 = 0$. $\delta \neq 0$. 10

5 Typical values of C_1, dashed line, and $\int^x C_1(s)ds$, versus x, for a flat bottom. 17

6 Typical values of C_3, dashed line, and $\int^x C_3(s)ds$, versus x, for a flat bottom. 18

7 Detuning parameter dependence on ω_1 and β for the water wave problem. 19

8 Phase plane for A_2 for $\delta \sim 0$. X axis is vertical. 20

9 Phase plane for A_2 for $\delta/2E_0^{1/2} \ll 1$. X axis is vertical. 22

10 Phase plane for A_2 for $\delta/2E_0^{1/2} \gg 1$. X axis is vertical. 23

11 $|a_2|^2$ dependence on the detuning parameter. In all cases $|a_1|^2(x = 0) = 1$. The interaction length and the power transferred to $|a_2|^2$ decreases as ΔQ increases. 26

12 Interaction length dependence on the nonlinear parameter ΔQ. The detuning parameter is scaled so that as $\Delta Q \to 0$, $m \to 1$. 27

13 Interaction length dependence on the nonlinear parameter α. 28

14 Interaction length dependence on the dispersion parameter β. . . . 29

15 Plot of K_5/α versus the fundamental frequency ω_1, and β for the water wave problem. 39

16 Plot of K_6/α versus the fundamental frequency ω_1, and β for the water wave problem. 39